Probing the Impedance of a Biological Tissue with PEDOT:PSS-Coated Metal Electrodes: Effect of Electrode Size on Sensing Efficiency

Dimitrios A. Koutsouras, Leona V. Lingstedt, Katharina Lieberth, Jonas Reinholz, Volker Mailänder, Paul W. M. Blom, and Paschalis Gkoupidenis*

Electrodes coated with poly(3,4-ethylenedioxythiophene):polystyrene sulfonate (PEDOT:PSS) have been employed to measure the integrity of cellular barriers. However, a systematic experimental study of the correlation between tissue integrity and impedance of the sensing device has not yet been conducted. Using impedance spectroscopy, how the impedance ratio of the biological tissue to the recording device affects the recording ability of the latter is investigated. PEDOT:PSS-coated electrodes of various dimensions are employed and the effect of their size to their sensing efficiency is examined. The biotic/abiotic ensemble is modeled with a simple equivalent circuit and an analytical expression of the total impedance as a function of frequency is extracted. The results reveal a critical impedance ratio of the biological tissue to the sensor which allows for efficient sensing of the tissue integrity. This work provides the ground rules for improved impedance-based biosensors with optimized sensitivity.

Organic electronic materials are currently the most promising candidates to revolutionize the field of bioelectronics. This view is justified by the unique set of features they possess and which allows them to interact with biological systems in an extremely effective way.[1] Conducting polymers in particular, have been widely exploited lately in biological-driven applications as electrode coatings as well as the channel material of organic-based transistors.[2] The reason behind that is their characteristic to improve the tissue/recording site interaction in vitro and also in vivo, by lowering the overall device impedance.[3] This is mainly due to their ability to conduct both ions and electrons, a fact which delivers extremely high capacitance values.[4] The above attributes have already resulted in a variety of applications spanning from neural interfacing,[5] biosensing,[6] and drug delivering[7] to the

materialization of neuromorphic devices[8] and electronic plants.[9] In addition, they offer a biocompatible substrate which favors the biotic/abiotic interplay[10] and a facile/cost-effective fabrication process that comes hand to hand with their solution-based manipulation. More than that, features like the above have also been widely exploited in the past for examining the integrity state of various types of tissue layers.

In general, epithelial and enthothelial cells form layers by accomplishing intercellular junctions between them and separating the apical (luminal) from the basolateral (abluminal) domain.[11] Most importantly, they are able to form a functional barrier among different compartments by controlling the passage of chemical compounds, nutrition ingredients, water molecules, and even cells through them.[12] This control can take place either along the formed tight junctions (paracellular pathway) or via transport through the cell cytoplasm (intracellular pathway).[11] The integrity of the barrier monolayer is, therefore, essential for assuring the physiological function of different compartments, and its loss signifies pathophysiological issues serving at the same time as a disease indicator. In addition, being able to accurately, fast, and easily monitor the level of this integrity is of great importance now more than ever. Namely, it allows for reliable tests on drug toxicity in in vitro models, especially since the 3Rs (Replacement, Reduction, Refinement) principle has become a necessity.[13] In practice, in order for the above integrity to be studied, the response of the tissue is usually tested taking under consideration the two ways that ions, molecules, and ingredients can pass through a biological cell layer, the intercellular and the paracellular pathway.[12]

Regarding the intercellular pathway, the cell membrane permeability is typically assessed by radiolabeled markers or nonradioactive fluorescence labeled proteins.[14] The paracellular one on the other hand, is commonly studied via transepithelial electrical resistance (TEER) measurements.[14] However, the former technique suffers from tracer compounds/barrier interferences, while the latter comes along with temporal resolution and reproducibility issues, in addition to a destructive effect on both cells and electrodes.

Consequently, alternative, noninvasive ways to check tissue integrity have been developed. Impedance spectroscopy (IS), in particular, is an automated and reliable way to improve TEER

Dr. D. A. Koutsouras, Dr. L. V. Lingstedt, K. Lieberth, Dr. J. Reinholz, Prof. V. Mailänder, Prof. P. W. M. Blom, Dr. P. Gkoupidenis
Max Planck Institute for Polymer Research
Ackermannweg 10, 55128 Mainz, Germany
E-mail: gkoupidenis@mpip-mainz.mpg.de

**ADVANCED
SCIENCE NEWS**

www.advancedsciencenews.com

**ADVANCED
HEALTHCARE
MATERIALS**

www.advhealthmat.de

measurements. It is based on defining the impedance (magnitude $|Z|$ and phase φ) of the tissue by sweeping a small AC voltage signal over frequency and recording the resulting AC current signal. Importantly, it allows for a system to be properly modeled due to the fact that except from the resistance provides information regarding the capacitance of the cell layer over a frequency range. Conducting polymers have proved to be a valuable asset in this task as their unique features allow the fabrication of state-of-the-art passive electrode devices. Indeed, a lot of studies have been, already, focused on ion transport through lipid bilayers and barrier tissues with the use of poly(3,4-ethylenedioxythiophene):polystyrene sulfonate (PEDOT:PSS) as the active material in the measuring device.[15] This is due to the fact that PEDOT:PSS has high conductivity, is commercially available, electrochemically stable, and can be easily processed into films from solution. It also presents many biologically desired features such as biocompatibility, stability in a wide pH range, as well as under physiological conditions. Notably, they can be used as electrode coatings facilitating the electrolyte/recording site interface throughout the measurements.

Organic electrochemical transistors (OECTs), on the other hand, are devices that consist of a degenerately doped conducting polymer film channel in contact with an electrolyte.[16] The swelling of the channel material yields high transconductance values for low operation voltages. As shown in previous studies,[15b,17] the presence of the tissue layer on a suspended filter (Transwell) affects the way the current in the channel is modulated by the gate electrode. As a result, the device constitutes not only a low-cost biosensor but also a candidate for the fabrication of diagnostic tools with high sensitivity and with the advantage of high temporal resolution. Interestingly, in these experiments the study of the cell layer integrity was facilitated by the decrease in the tissue area with the use of an insulator (silicone).[15b] Despite the fact that silicone was employed manually and without optimal control of the final area, its presence was imperative for the measurements. This is due to the fact that the ensuing increase of the tissue impedance compared to the one of the measuring device plays a crucial role in the biosensor function. In a following theoretical study, the biological barrier layer-functionalized OECT was modeled.[18] The result showed that the barrier-to-device area ratio is an important parameter in order to tune the device sensitivity and to define the detection limit. The biosensor/tissue structure as a whole was modeled with a five-element circuit, without though any experimental validation. Later on, in a different study, the scaling of the impedance of conducting polymer-coated electrodes as a function of area, film thickness, and electrolyte concentration was examined revealing a universal scaling rule for the above mentioned parameters.[19] Nevertheless, up to now, there is no systematic experimental investigation of the device efficiency to sense the tissue integrity, as a function of the ratio between the impedance of the tissue and that of the measuring device.

In this work, we examine the effect of the impedance ratio λ of a tissue cell layer to the measuring electrode on the sensing ability of the later, by means of frequency domain electrochemical impedance spectroscopy. The study is conducted by systematically changing the area of the electrode, a fact reflected on its impedance spectrum. The results show that for a specific
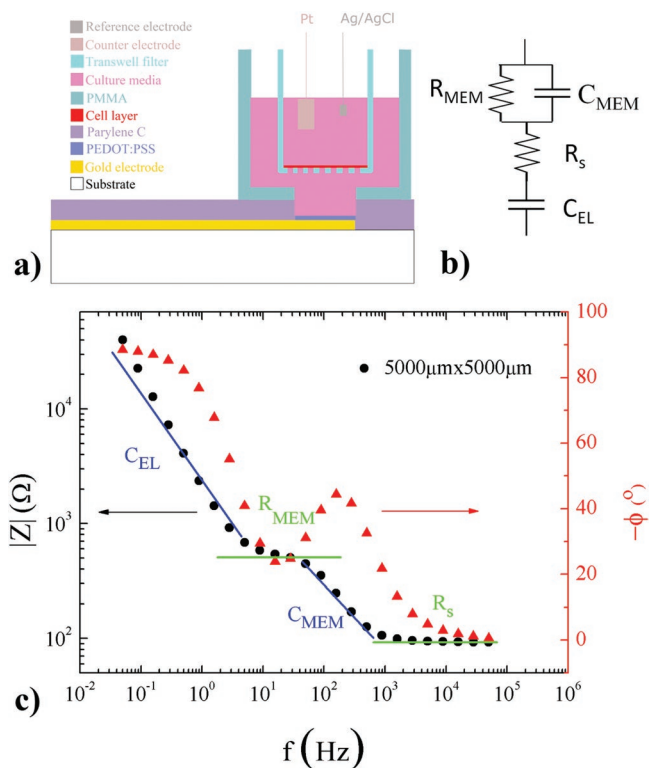

Figure 1. Experimental setup and electrode impedance spectrum. a) Schematic that represents the Transwell filter on top of the PEDOT:PSS-coated gold electrode. The filter hosts the CaCo-2 cell layer allowing for electrochemical impedance measurements to take place. b) The equivalent circuit models the system taking into account a R_{EL}–C_{EL} circuit which corresponds to the electrode and a R_{MEM}//C_{MEM} circuit which corresponds to the tissue layer. In this cartoon, R_{EL} is the spreading resistance at the electrode/electrolyte interface and C_{EL} is the capacitance at the same interface. R_{MEM} is the resistive part of the biological membrane while C_{MEM} its capacitance. c) Electrode impedance spectrum. The modeled resistors and capacitors used in the equivalent circuit are present in the impedance spectrum of the 5000 µm × 5000 µm electrode (Bode magnitude $|Z|$ and phase φ plots). C and R notations are used to signify the capacitive and resistive nature of the impedance at those frequency regions.

ratio λ, a well-documented in literature plateau appears.[18,20] This plateau is attributed to the impedance of the tissue layer. By changing λ, the plateau disappears confirming that there is a critical value above which we can achieve sensing. The total biotic/abiotic ensemble can be described by a simple four-element circuit following a previous work.[19] The minimum use of electrical elements leads to an easy extraction of analytical formulas for the frequency-dependent impedance Z as a function of geometrical characteristics. Since the study targets the PEDOT:PSS film features, its outcome is valid for both conducting polymer coated electrodes and OECTs, as the extrapolation from the former device to the latter is straightforward. Our results pave the way for better understanding the necessary conditions for biosensing device optimization, in order to minimize the mismatch between electronics and biological tissue.

Figure 1a represents the experimental setup. A poly(methyl methacrylate) (PMMA) chamber was initially constructed and then glued on the electrode device in order to encompass its active area. A compartment is thus created to host a Transwell
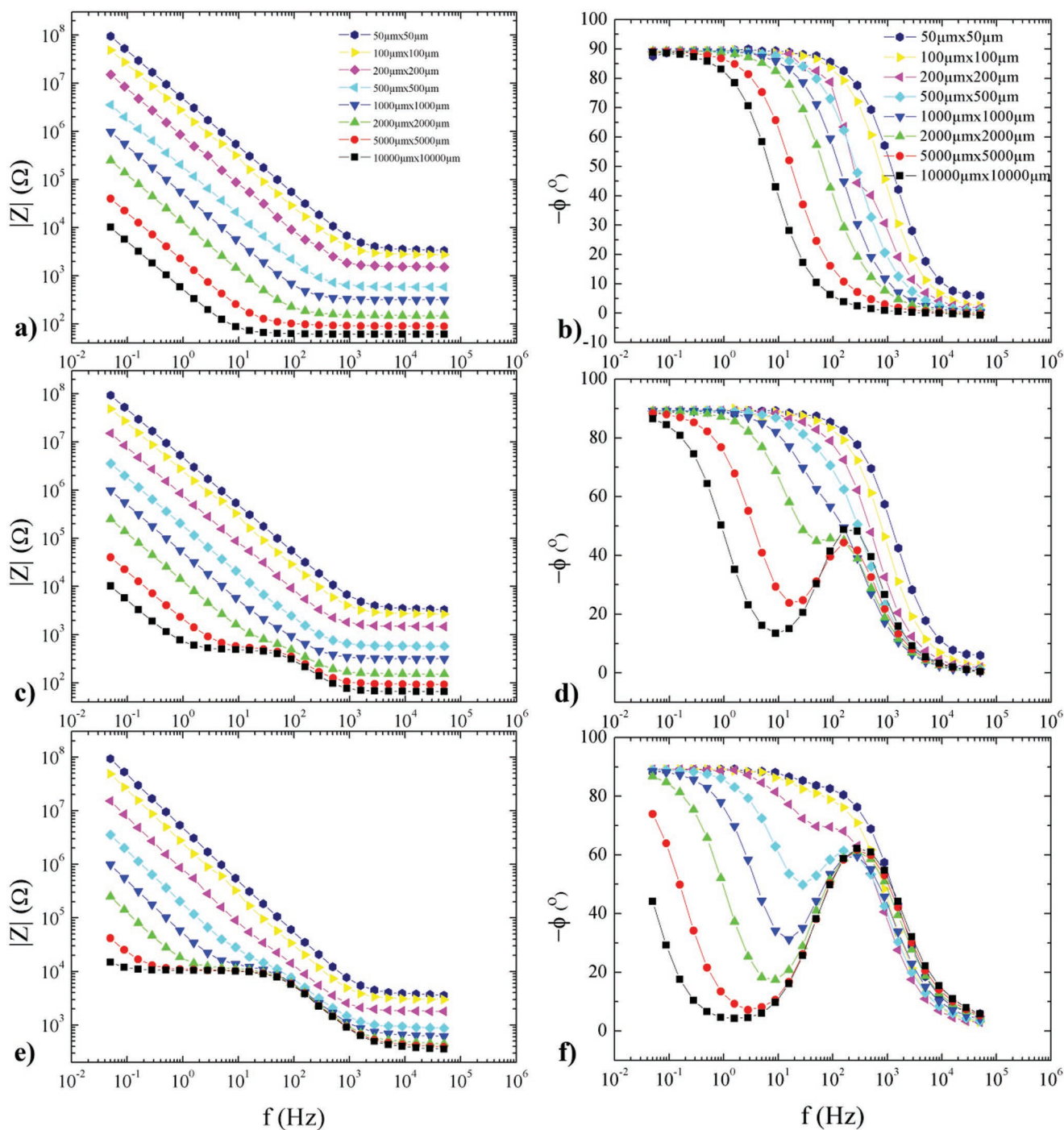
Figure 2. Bode magnitude and phase spectra of electrodes of various sizes with and without cells. a,b) Impedance plots (Bode magnitude |Z| and phase φ, respectively) of PEDOT:PSS-coated gold electrodes of various sizes. c,d) The presence of the cell barrier alters the shape of the spectra with the appearance of a plateau in the Bode magnitude and a peak in the phase plots of the electrodes with the smaller impedance (greater sized electrodes). e,f) By changing the effective area of the cell barrier tissue (with the use of PDMS) even smaller sized electrodes can be recruited to sense the presence of the biological tissue.

filter on which the cells were cultured (see also the Experimental Section). The chamber is filled with Eagle's minimum essential medium (EMEM), a culture medium that establishes an ionic connection between the recording sites (electrodes) and the biological tissue. A useful way to study the ensemble

is to represent the system as an equivalent electrical circuit like the one presented in Figure 1b and which has been widely used throughout literature.[11] The electrode is simulated by a basic R_s–C_{EL} circuit in series with a basic $R_{MEM}//C_{MEM}$ circuit. R_s is the spreading resistance which depends on the electrode's

ADVANCED
SCIENCE NEWS
www.advancedsciencenews.com

ADVANCED
HEALTHCARE
MATERIALS
www.advhealthmat.de

size[21] and C_{EL} represents the capacitor created at the electrode interface with the electrolyte. R_{MEM} on the other hand expresses the ohmic resistance of the paracellular pathway due to the presence of tight junctional proteins connecting the cells. This is approximately the ohmic resistance that can also be obtained via TEER measurements considering the fact that $R_s \ll R_{MEM}$. Finally, C_{MEM} is the electrical capacitance of the biological membrane. In the extreme case that the membrane integrity is completely lost, the circuit degenerates to a R_s–C_{EL} circuit which corresponds to the electrode without the presence of any cell on top.

In Figure 1c, a reference example of the impedance spectroscopy spectrum of a 5000 µm × 5000 µm electrode under the presence of the cell layer is shown. In the plot, four distinctive regions are clearly presented. At very high frequencies, the system exhibits a resistive behavior with a constant R_s value over frequency. For smaller frequencies (10^2–10^3 Hz), a capacitive part becomes dominant corresponding to the capacitance of the tissue C_{MEM}, followed by a second resistive part R_{MEM} from 1 to 10^2 Hz due to the paracellular resistance this time. For this particular Caco-2 cell barrier, the fitted R_{MEM} value equals to 400 Ω which is close to the experimentally measured TEER value of 425 Ω. It is worth noticing here that the R_{MEM}//C_{MEM} combination of the equivalent circuit represents the biological part of the system. Most importantly, its footprint on the spectrum, with the form of a plateau, validates the ability of the electrode to sense the tissue barrier presence. Finally, below 1 Hz we return to a capacitive regime having the formed capacitor C_{EL} at the medium/coated electrode interface being the dominant circuit element. In the same figure, the corresponding phase is also presented. Studying the data from a complementary perspective, the resistive nature of the system is clear through the zero phase φ value at high frequencies. The presence of the tissue capacitance becomes apparent with the phase peak between 10^2 and 10^3 Hz, while the tissue resistance emerges from 1 to 10^2 Hz. Below that frequency, the capacitance of the electrode dominates with a phase value φ that approaches −90°.

The above described impedance features of the interaction between the tissue and the electrode are better depicted in **Figure 2**. Figure 2a illustrates typical impedance spectra of electrodes with various areas and with no membrane on them (reference experiment) and Figure 2b presents the corresponding phase. The resistive part at the higher frequencies and the capacitive part at the lower ones are clearly portrayed for every electrode. Briefly, it can be concluded that a change on the electrode area alters the position of the corresponding curve in the impedance magnitude |Z|–f plane, leaving yet, unchanged its overall shape. This scaling behavior is in agreement with previous work.[19] Nonetheless, the presence of the Caco-2 barrier tissue layer modifies the electrical characteristics of the system, a fact reflected on the impedance spectra presented in Figure 2c. While a change is unseen for the smaller electrodes (sizes 1000 µm × 1000 µm and below), it is apparent for the larger ones (sizes 10 000 µm × 10 000 µm and 5000 µm × 5000 µm). Moreover, there seems to be a transition electrode size separating the two extreme cases (non-sensing and sensing electrodes). This observation implies a connection between the recording site area and consequently its impedance

(here the experimentally accessible parameter is the variation of electrode area through fabrication), and its ability to sense the presence of the cell layer above it.[18] During the measurement, a small amplitude AC signal is applied between the Ag/AgCl reference electrode and the working electrode (PEDOT:PSS-coated electrode). This small AC voltage perturbation creates an AC current that is recorded by the working electrode. By scanning the AC frequency, the impedance spectrum of the electrode over a frequency range is obtained. Naturally, the presence of the tissue barrier impedes the ionic charge movement. Whether the electrical fingerprint of the tissue will eventually be recorded or not, depends on the ratio between the impedance attributed to the layer and the one attributed to the electrode. Larger electrodes are better in capturing the transmitted signal due to their small impedance compared to the cell layer one. This fact is depicted on the plateau shown for frequencies below 100 Hz for these electrodes. Similarly, regarding the impedance phase φ spectra, peaks are also observed for them in Figure 2d. These peaks denote the capacitive contribution due to the presence of the cell membrane.

Having the above in mind, it can be concluded that the impedance spectrum is affected by the values of the electric components of the equivalent circuit. What that means is that if we are to change the values of either R_s, C_{EL} that correspond to the electrode or R_{MEM}, C_{MEM} that correspond to the biological tissue, different traces will be obtained.[11] This is illustrated in Figure 2e where polydimethylsiloxane (PDMS) was used on the back side of the filter in order to reduce its size to ≈90% of the initial area (Experimental Section), before Caco-2 cells were cultured on it. In terms of the electric circuit components, that results in an increased R_{MEM} value with a simultaneous decreased capacitance C_{MEM} leading to an overall impedance increment of the R_{MEM}//C_{MEM} part of the circuit. As a result, more electrodes of the used electrode set, will be able to sense the presence of the cell layer leading to the conclusion that the ratio λ of |Z_{MEM}| to |Z_{EL}| plays a crucial role in the biosensing abilities of the device. Indeed, Figure 2e depicts the increase in the number of electrodes that present the impedance magnitude plateau attributed to the cell presence. Similarly, Figure 2f shows the phase spectra with more electrodes presenting a peak due to the existence of the tissue layer.

Most importantly, there seems to be a critical impedance ratio value |Z_{MEM}|/|Z_{EL}| that signifies the transition from the non-sensing regime (that corresponds to the smallest electrode, size 50 µm × 50 µm) to the sensing regime (that corresponds to the greatest electrode, size 10 000 µm × 10 000 µm). In particular, **Figure 3**a reveals that for the 50 µm × 50 µm electrode (non-sensing regime) there is no obvious difference between the impedance spectrum with and without the presence of cells. This implies that the biological tissue is literately invisible to the biosensor. Figure 3b, on the other hand, illustrates that for the 10 000 µm × 10 000 µm electrode (sensing regime) the situation changes drastically since the presence of the tissue dramatically alters the electrode's spectrum.

In order to determine the transition requirement, an analytical formula for estimating the impedance magnitude |Z| as a function of frequency f was derived based on the four-element equivalent circuit presented in Figure 1b. The formula provides the impedance magnitude |Z| and the corresponding phase φ for

**ADVANCED
SCIENCE NEWS**

www.advancedsciencenews.com

**ADVANCED
HEALTHCARE
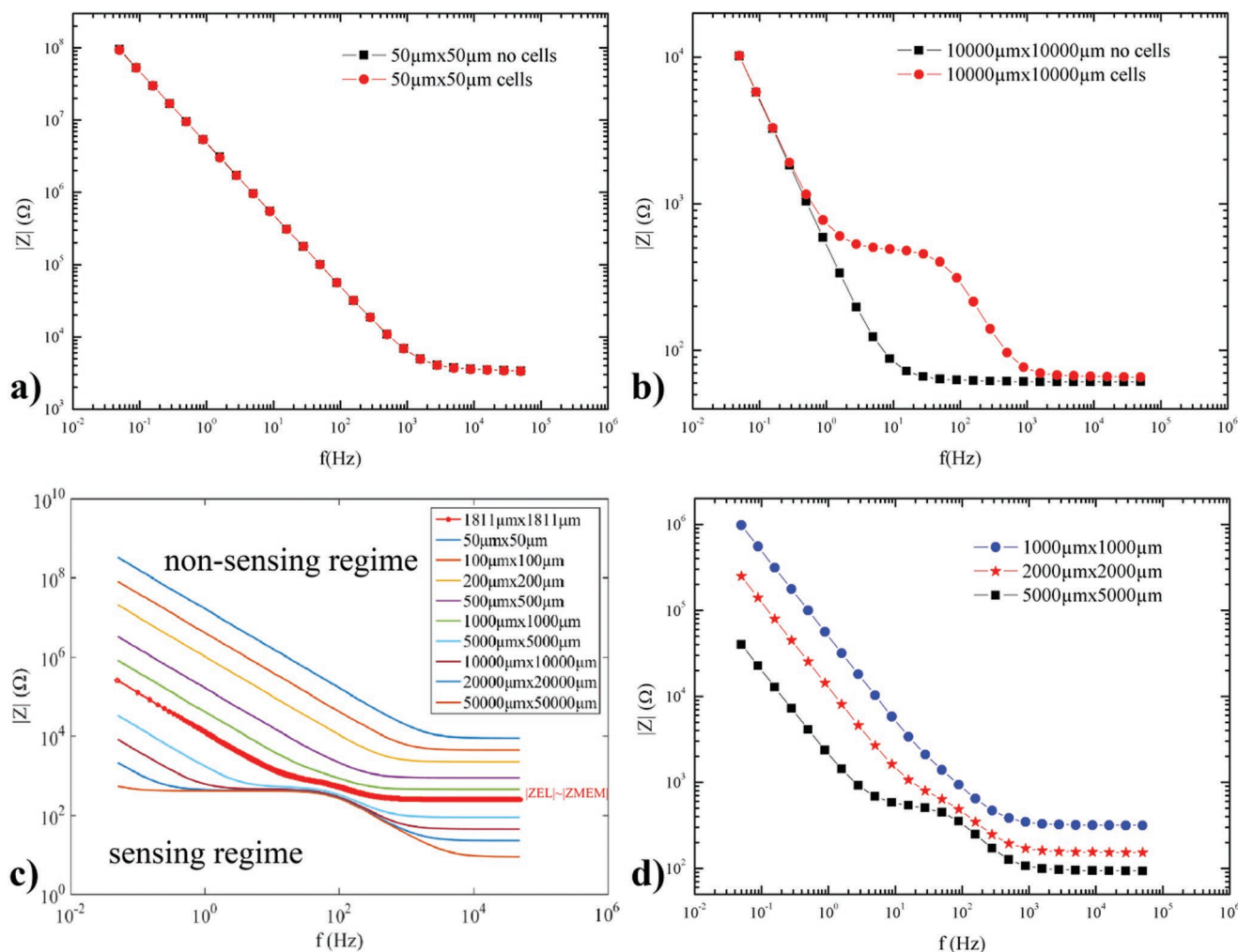MATERIALS**

www.advhealthmat.de

Figure 3. Experimental measurements and simulation of the impedance magnitude |Z| of various sized electrodes over frequency. a) The impedance spectrum of the smallest used electrode (50 µm × 50 µm) remains virtually unaffected by the presence of the cell layer. b) Nevertheless, the presence of the tissue has an obvious effect on the greatest used electrode (10 000 µm × 10 000 µm) as it alters noticeably its impedance spectrum. c) Simulation of the impedance spectra of the tissue barrier/electrode ensemble for various electrode sizes with the use of Equation (1). While the impedance magnitude of the electrode $|Z_{EL}|$ is greater than that of the tissue barrier $|Z_{MEM}|$ the latter is virtually invisible to the former. For $|Z_{EL}|$ smaller than $|Z_{MEM}|$ a plateau emerges. The value of this plateau corresponds to the TEER obtained cell resistance R_{MEM}. The transition from the nonsensing to the sensing regime goes through an electrode size with impedance value $|Z_{EL}|$ almost equal to $|Z_{MEM}|$ (transition electrode size). The estimated non-sensing value of the electrode size that satisfies this equality is about 1800 µm (Supporting Information). d) Experimental data that support the above. The 2000 µm × 2000 µm electrode has a size that satisfies the impedance ratio requirement ($\lambda \approx 1$) for the transition from the nonsensing (1000 µm × 1000 µm) to the sensing (5000 µm × 5000 µm) electrode.

different electrode sizes α and different PEDOT:PSS thicknesses t (Supporting Information). For the impedance magnitude |Z|

$$|Z| = \sqrt{\left(\frac{\rho \ln 4}{\pi a} + \frac{R_{MEM}}{1+\left(2\pi f R_{MEM} C_{MEM}\right)^2}\right)^2 + \left(\frac{1}{2\pi f C^* a^2 t} + \frac{2\pi f R_{MEM}^2 C_{MEM}}{1+\left(2\pi f R_{MEM} C_{MEM}\right)^2}\right)^2}$$

(1)

while the phase φ is

$$\varphi = \tan^{-1}\left(\frac{\dfrac{1}{2\pi f C^* a^2 t} + \dfrac{2\pi f R_{MEM}^2 C_{MEM}}{1+\left(R_{MEM} C_{MEM} 2\pi f\right)^2}}{\dfrac{\rho \ln 4}{\pi a} + \dfrac{R_{MEM}}{1+\left(R_{MEM} C_{MEM} 2\pi f\right)^2}}\right)$$

(2)

where ρ is the solution resistivity, α the side of the square electrode, t the PEDOT:PSS film thickness, f the frequency, C^* the capacitance per volume of the conducting polymer (PEDOT:PSS in our case), R_{MEM} the ohmic resistance of the tissue layer, and C_{MEM} the capacitance of the tissue cell layer. For this particular study (i.e., for a given tissue), the degrees of freedom can be narrowed down to 2, that is, the electrode side α and the film thickness t, since for Caco-2 cell layers the values for the resistance and the capacitance are $R_{MEM} = 400 \ \Omega$ and $C_{MEM} = 5 \times 10^{-6} \ F$, respectively, as obtained from fitting to experimental measurements as well as from data in literature (for details regarding the impedance spectrum of the membrane, refer to Figure S2, Supporting Information).[14] The capacitance per volume C^* of PEDOT:PSS has already been

estimated to 39 F cm^{-3}. Therefore, Figure 3c plots the impedance magnitude $|Z| - f$ for different electrode dimensions based on Equation (1). The PEDOT:PSS film thickness was kept fixed at $t = 100$ nm. The simulated results show that there is a curve (signified by the red stars) which divides the $|Z| - f$ plane in two regimes. In the upper regime where $|Z_{MEM}| < |Z_{EL}|$, the curves resemble the typical curves of PEDOT:PSS electrodes in an electrolyte solution. In particular, a high-frequency resistive part and a lower frequency capacitive part constitute the plot with no evidence of the tissue shown. In the lower regime though, where $|Z_{MEM}| > |Z_{EL}|$, the curves exhibit a characteristic plateau which corresponds to the presence of the Caco-2 layer. In addition, the transition between these regions takes place for an electrode with impedance magnitude value similar to the one of the biological tissue barrier $|Z_{MEM}| \approx |Z_{EL}|$.

Consequently, the necessary condition for tuning the device sensing ability should be

$$|Z_{MEM}| \geq |Z_{EL}| \tag{3}$$

$$\lambda = \frac{|Z_{MEM}|}{|Z_{EL}|} \geq 1 \tag{4}$$

For the under study system, the function of the absolute difference between the impedance magnitude of the tissue and the electrode $||Z_{MEM}| - |Z_{EL}||$ presents a minimum value in a logarithmic plot and for a size of ≈ 1800 µm (Figure S1, Supporting Information). Greater sized electrodes are able to successfully sense the biological tissue while smaller ones are not. The above are further supported by the experimental measurements in Figure 3d. The impedance spectra of electrodes of different sizes, and consequently of different impedance magnitude values, are presented showing that the ratio λ should be greater than 1 in order for the electrode to be able to record. In particular, when $|Z_{MEM}| < |Z_{EL}|$ (1000 µm × 1000 µm electrode) the tissue barrier layer is not detectable. A critical point appears for the 2000 µm × 2000 µm electrode due to the fact that for this size $|Z_{MEM}| \approx |Z_{EL}|$. Finally, for $|Z_{MEM}| > |Z_{EL}|$ (5000 µm × 5000 µm electrode) the system is properly tuned and consequently able to sense the presence of the cells. Furthermore, the sensitivity of the optimized electrode is practically independent of the electrode area, given that an area larger than the critical value is used (Figure S3, Supporting Information).

In conclusion, in this work we studied how the impedance ratio, $\lambda = |Z_{MEM}|/|Z_{MEM}|$, between a biological tissue and an electrode biosensor affects the sensing ability of the latter. The analysis was conducted with the help of impedance spectroscopy while the impedance of the sensing device was systematically changed by varying its size. The presence of the tissue barrier was confirmed with the appearance of a plateau as expected by the literature. A simple four-element circuit $R_s - C_{EL} - R_{MEM}//C_{MEM}$ was proved adequate to model the system resulting in an analytical formula for the impedance as a function of frequency. The impedance magnitude for different electrode areas was simulated over frequency and revealed a transition from a nonsensing to a sensing regime. Critical parameter for this transition is the ratio λ as it turned out that for values of the electrode impedance $|Z_{EL}|$ greater than the values of the tissue layer impedance $|Z_{MEM}|$ the electrodes did not present any

biosensing competence. As $|Z_{EL}|$ decreased, due to the increase of their area, the electrodes disclosed their recording ability exactly when their impedance became smaller than the one of the tissue cell barrier. Therefore, a λ value greater than 1 should be targeted for improved biosensing efficiency. Importantly, as the $R_s - C_{EL}$ equivalent circuit models both PEDOT:PSS-coated electrodes and OECTs of the same film thickness, this conclusion is valid for both these devices. It should be mentioned that figures of merit for conducting polymers, such as volumetric capacitance of PEDOT:PSS, are the same when extracted from impedance spectroscopy measurements both in passive electrodes and OECTs.[19] In addition, the results can also be generalized for the evaluation of the integrity of any other type of cell layer (see also Figure S3, Supporting Information). This work provides guidelines for the design of impedance-based sensors and for the optimization of their sensing ability. In addition, our findings highlight the pivotal role of PEDOT:PSS-coated electrodes can play in the future of the biomedical field. Their importance derives from the useful set of features conducting polymers can offer (biocompatibility, facile processing, low-cost fabrication). Many challenges, mostly in gaining a deeper understanding on the fundamental phenomena that govern the material structure and the material/electrolyte interface are still to be tackled. Nevertheless, PEDOT:PSS is an excellent candidate which promise to recast bioelectronics.

Experimental Section

Device Fabrication: The devices were fabricated using standard microfabrication techniques. Initially, the substrates, 26 mm × 76 mm microscope glass slides, were thoroughly cleaned first in a soap (Micro-90) and then in a 1:1 (vol vol^{-1}) solvent mixture (acetone/isopropanol) sonication bath. The gold electrodes were patterned with the use of photoresist (S1813) and an initial photolithography step, just before a double layer of Parylene C was employed to encapsulate the device. Between the two layers of Parylene C, soap solution (Micro-90, 1% vol vol^{-1} in bidistilled water) served as an antiadhesive layer, facilitating a later peel-off step of the fabrication. On the other hand, silane A-174 (gamma-mehtacryloxypropyltrimethoxysilane) purchased from SCS, an adhesion promoter, was deployed between the substrate and the first Paralyne C layer in order for the adhesion to be enhanced. On top of the second Parylene C layer, a different photoresist (AZ 9260) was spun and a second photolithography step defined window openings on the photoresist above each electrode. Reactive ion etching (RIE) with O$_2$ plasma was used to remove Parylene C under those window openings and to expose the active area of each one of them. PEDOT:PSS was afterward spun creating a thin film of a conducting polymer of around 100 nm on the device. A final peel-off step defined the active area of the conducting polymer coated gold electrodes. The devices were subsequently hard baked for an hour at 140 °C before placed in bidistilled water overnight for the removal of the excess of any low molecular weight molecules. PEDOT:PSS formulation: 38 mL of PEDOT:PSS aqueous dispersion (Clevios PH-1000), 2 mL of ethylene glycol (conductivity enhancement), 50 µL of 4-dodecylbenzenesulfoonic acid (DBSA) (film formation), and 0.4 mL of 3-methacryloxypropyl-trimethoxysilane (GOPS) (surface adhesion promoter and polymer cross-linking agent).

Cell Culture: Caco-2 cells were seeded at 1.5 × 10^5 (cells/insert) on Transwell filters with an area of 1.12 cm^2 and pore size of 0.4 µm. The cells were cultured in EMEM (Invitrogen) with 10% fetal bovine serum (FBS, Invitrogen), 2 × 10^{-3} M glutamine (GlutaMax-1, 100×, Invitrogen), and Pen-strep (10 000 U mL^{-1} penicillin, 10 000 µg mL^{-1} streptomycin, Invitrogen) at 37 °C in a humified atmosphere with 5% CO$_2$ with medium

**ADVANCED
SCIENCE NEWS**

www.advancedsciencenews.com

**ADVANCED
HEALTHCARE
MATERIALS**

www.advhealthmat.de

changes every 2–3 d. The cell filters were used after 14 d with a TEER of 476 Ω cm^2, showing a closed cell layer. For an increased cell layer resistance, the area was reduced to ≈0.08 cm^2 by applying PDMS on the back side for the filter. In case of PDMS-modified Transwell filters, an additional collagen coating was implemented for improved cell attachment.

Device Characterization and Measurements: The impedance spectroscopy measurements were realized in a potentiostat/galvanostat (µAUTOLAB TYPE III). For the measurements, Transwell filters were used to host the Caco-2 layer of cells above the recording sites. During the experiment, the PEDOT:PSS-coated electrodes served as the working electrode in a three-electrode configuration setup. Ag/AgCl and Pt electrodes were the reference and the counter electrode, respectively. The electrodes were fabricated, characterized, and used to perform the experiments with the biological tissue within a timescale of five months. Moreover, endurance measurements were performed for ≈5 h and practically showed no degradation of the conducting polymer (Figure S4, Supporting Information). TEER measurements were realized with a handheld volt-ohm meter EVOM2TM from World Precision Instruments, assessing the integrity of the cellular barrier by measuring the ohmic resistance. The EndOhm chamber consists of two concentric electrodes incorporating a voltage-sensing Ag/AgCl pellet in the center and an annular current electrode. By applying a small AC signal across two electrode plates, which are placed on both sides of a cell monolayer and measuring the voltage and current, the electrical resistance is calculated. The TEER is given in Ω cm^2, normalized on the area of the Transwell insert.

Data Analysis: The data were analyzed and plotted using Matlab software (Mathworks) and Origin Ltd. For the impedance magnitude and phase as a function of frequency simulations, Matlab code was written with values $R_{MEM} = 400$ Ω and $C_{MEM} = 5 \times 10^{-6}$ F for the capacitance and resistance of the Caco-2 cell layer, respectively.

Supporting Information

Supporting Information is available from the Wiley Online Library or from the author.

Conflict of Interest

The authors declare no conflict of interest.

Keywords

[1] a) M. Berggren, A. Richter-Dahlfors, *Adv. Mater.* **2007**, *19*, 3201; b) J. Rivnay, R. M. Owens, G. G. Malliaras, *Chem. Mater.* **2014**, *26*, 679; c) T. Someya, Z. Bao, G. G. Malliaras, *Nature* **2016**, *540*, 379.

[2] a) G. Wallace, G. Spinks, *Soft Matter* **2007**, *3*, 665; b) A. Blau, A. Murr, S. Wolff, E. Sernagor, P. Medini, G. Iurilli, C. Ziegler, F. Benfenati, *Biomaterials* **2011**, *32*, 1778; c) D. Khodagholy, T. Doublet, P. Quilichini, M. Gurfinkel, P. Leleux, A. Ghestem, E. Ismailova, T. Hervé, S. Sanaur, C. Bernard, G. G. Malliaras, *Nat. Commun.* **2013**, *4*, 1575; d) D. C. Martin, *MRS Commun.* **2015**, *5*, 131.

[3] a) X. Cui, D. C. Martin, *Sens. Actuators, B* **2003**, *89*, 92; b) R. Green, M. R. Abidian, *Adv. Mater.* **2015**, *27*, 7620; c) C. Bodart, N. Rossetti, J. E. Hagler, P. Chevreau, D. Chhin, F. Soavi, S. B. Schougaard, F. Amzica, F. Cicoira, *ACS Appl. Mater. Interfaces* **2019**, *11*, 17226.

[4] D. C. Martin, G. G. Malliaras, *ChemElectroChem* **2016**, *3*, 686.

[5] a) D. A. Koutsouras, A. Hama, J. Pas, P. Gkoupidenis, B. Hivert, C. Faivre-Sarrailh, E. Di Pasquale, R. M. Owens, G. G. Malliaras, *MRS Commun.* **2017**, *7*, 259; b) J. Pas, C. Pitsalidis, D. A. Koutsouras, P. P. Quilichini, F. Santoro, B. Cui, L. Gallais, R. P. O'Connor, G. G. Malliaras, R. M. Owens, *Adv. Biosyst.* **2018**, *2*, 1700164.

[6] N. Y. Shim, D. Bernards, D. Macaya, J. DeFranco, M. Nikolou, R. Owens, G. Malliaras, *Sensors* **2009**, *9*, 9896.

[7] D. T. Simon, S. Kurup, K. C. Larsson, R. Hori, K. Tybrandt, M. Goiny, E. W. H. Jager, M. Berggren, B. Canlon, A. Richter-Dahlfors, *Nat. Mater.* **2009**, *8*, 742.

[8] a) P. Gkoupidenis, N. Schaefer, B. Garlan, G. G. Malliaras, *Adv. Mater.* **2015**, *27*, 7176; b) P. Gkoupidenis, D. A. Koutsouras, G. G. Malliaras, *Nat. Commun.* **2017**, *8*, 15448.

[9] E. Stavrinidou, R. Gabrielsson, E. Gomez, X. Crispin, O. Nilsson, D. T. Simon, M. Berggren, *Sci. Adv.* **2015**, *1*, e1501136.

[10] a) R. T. Richardson, B. Thompson, S. Moulton, C. Newbold, M. G. Lum, A. Cameron, G. Wallace, R. Kapsa, G. Clark, S. O'Leary, *Biomaterials* **2007**, *28*, 513; b) M. R. Abidian, J. M. Corey, D. R. Kipke, D. C. Martin, *Small* **2010**, *6*, 421.

[11] K. Benson, S. Cramer, H.-J. Galla, *Fluids Barriers CNS* **2013**, *10*, 5.

[12] M. S. Balda, J. A. Whitney, C. Flores, S. González, M. Cereijido, K. Matter, *J. Cell Biol.* **1996**, *134*, 1031.

[13] V. Y. Soldatow, E. L. LeCluyse, L. G. Griffith, I. Rusyn, *Toxicol. Res.* **2013**, *2*, 23.

[14] B. Srinivasan, A. R. Kolli, M. B. Esch, H. E. Abaci, M. L. Shuler, J. J. Hickman, *J. Lab. Autom.* **2015**, *20*, 107.

[15] a) D. A. Bernards, G. G. Malliaras, G. E. S. Toombes, S. M. Gruner, *Appl. Phys. Lett.* **2006**, *89*, 053505; b) L. H. Jimison, S. A. Tria, D. Khodagholy, M. Gurfinkel, E. Lanzarini, A. Hama, G. G. Malliaras, R. M. Owens, *Adv. Mater.* **2012**, *24*, 5919.

[16] D. A. Bernards, G. G. Malliaras, *Adv. Funct. Mater.* **2007**, *17*, 3538.

[17] a) S. A. Tria, L. H. Jimison, A. Hama, M. Bongo, R. M. Owens, *Biochim. Biophys. Acta, Gen. Subj.* **2013**, *1830*, 4381; b) S. Tria, L. H. Jimison, A. Hama, M. Bongo, R. M. Owens, *Biosensors* **2013**, *3*, 44.

[18] G. C. Faria, D. T. Duong, A. Salleo, C. A. Polyzoidis, S. Logothetidis, J. Rivnay, R. Owens, G. G. Malliaras, *MRS Commun.* **2014**, *4*, 189.

[19] D. A. Koutsouras, P. Gkoupidenis, C. Stolz, V. Subramanian, G. G. Malliaras, D. C. Martin, *ChemElectroChem* **2017**, *4*, 2321.

[20] J. Rivnay, M. Ramuz, P. Leleux, A. Hama, M. Huerta, R. M. Owens, *Appl. Phys. Lett.* **2015**, *106*, 043301.

[21] J. Newman, *J. Electrochem. Soc.* **1966**, *113*, 501.